Heliyon 10 (2024) e31019

Contents lists available at ScienceDirect

Heliyon

journal homepage: www.cell.com/heliyon

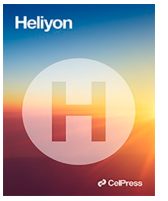

Research article

Experimental and numerical study of temperature evolution and hydrogen desorption process on an amorphous alloy $Mg_{50}Ni_{50}$

Chaker Briki [a,*], Maha M. Almoneef [b,**], Abdelhakim Settar [c], Mbarek Mohamed [d], Abdelmajid Jemni [a]

[a] University of Monastir, Faculty of Sciences, Laboratory of Thermal and Energetic Systems Studies, LR99ES31, 5019, Monastir, Tunisia
[b] Department of Physics, College of Science, Princess Nourah Bint Abdulrahman University, P.O. Box 84428, Riyadh, 11671, Saudi Arabia
[c] INSA Centre Val de Loire, Université Orléans, Prisme EA 4229, Bourge, F-18020, France
[d] Research Unit (UR 11ES55), New Materials and Organic Electronic Devices, Faculty of Science, University of Monastir, 5000, Tunisia

ARTICLE INFO

Keywords:
Amorphous alloy
$Mg_{50}Ni_{50}$
Desorption
Activation energy
Formation enthalpy
Formation entropy

ABSTRACT

In the present study, we explored the temperature evolution and hydrogen desorption properties of the $Mg_{50}Ni_{50}$ alloy through both numerical simulation and experimental analyses. Desorption kinetics characterization was carried out using the volumetric method, specifically employing a Sievert's-type apparatus to investigate solid-gas reactions. The experiments covered a temperature range from 313 K to 353 K, with an initial hydrogen pressure of 12 bar. Simultaneously, a mathematical approach was employed to numerically investigate the temperature evolution within the hydride bed. Using COMSOL Multiphysics as a simulator, a numerical simulation was conducted based on experimental data. The study examined the impact of cooling temperature on hydride temperature evolution. Results revealed that hydrogen desorption kinetics of the amorphous $Mg_{50}Ni_{50}$ alloy are more significant compared to those of Mg_2Ni compounds. Moreover, the effect of the warming temperature on the equilibrium pressure can also be observed in the hydrogen desorption isotherm curves. The experimental study of the $Mg_{50}Ni_{50}$ alloy provided activation energy data, along with determination of hydride formation enthalpy and entropy. On the other hand, we showed that the hydride temperature is maximum at the hydride-hydrogen interface within the hydride center.

1. Introduction

The utilization of hydrogen as an energy vector presents a crucial solution, addressing both the global energy demand and the imperative to replace current fossil fuels prevalent in diverse industrial applications. The primary prerequisite for hydrogen to emerge as a prominent energy source in the future lies in the advancement of technologies for its storage, production, and subsequent utilization. Metal and intermetallic hydrides offer a significant avenue for hydrogen storage, providing elevated storage density per unit volume and can be deemed safer when compared to traditional storage methods such as liquid or gaseous forms [1–3].

Recently, alloys designed for hydrogen storage represent materials with the ability to absorb and release a substantial amount of hydrogen in a reversible manner under specific temperatures and pressures. Within this category, magnesium-based compounds stand

* Corresponding author.
** Corresponding author.
E-mail addresses: chakerbriki@gmail.com (C. Briki), mmalmoneef@pnu.edu.sa (M. M. Almoneef).

https://doi.org/10.1016/j.heliyon.2024.e31019
Received 15 July 2023; Received in revised form 7 April 2024; Accepted 9 May 2024
Available online 15 May 2024

out as particularly promising materials for hydrogen storage, owing to their remarkable hydrogen capacity. Specifically, magnesium hydride (MgH_2) exhibits a notable hydrogen storage capacity of approximately 7.6 wt%, a significantly higher value compared to other alloys such as $LaNi_5$, which has a storage capacity of around 1.5 wt% [4–8]. However, Mg-based alloys exhibit specific properties related to their relatively modest kinetic reaction rates, elevated operating temperatures, and pressures.

In response to these challenges, many researchers have directed their efforts towards the development of alternative Mg-based alloys [9,10]. It is worth noting that Mg-based alloys do not readily react with hydrogen at near-ambient pressures and temperatures [11].

In the extensive exploration of Mg-based alloys conducted to date, despite occasional conflicting results in certain studies, specific elements have emerged as particularly promising due to their notable hydrogen storage capacity. Several experimental and theoretical investigations have delved into the hydrogen desorption characteristics of various Mg-based alloys [12–20]. Notably, Orimo et al. [21] focused on examining the H_2 storage properties of the $Mg_{50}Ni_{50}$ alloy in its amorphous state. Their findings indicated that the amorphous alloy exhibited the ability to absorb hydrogen up to a high concentration without undergoing a phase transition to a crystalline state. This is a significant observation because crystalline materials often exhibit limited hydrogen absorption capabilities and require higher temperatures and pressures to release hydrogen. Moreover, Benjamin et al. [22,23] have advocated for the application of a mechanical alloying (MA) process in the context of Mg-based materials. These methods facilitate the creation of fine-grained structures characterized by high surface areas, thereby enhancing the kinetics of hydrogen absorption and desorption. The augmented surface area provides more active sites for hydrogen to interact with the material, ultimately improving hydrogen storage performance. This technology contributes to the microstructural refinement of the alloy mesh [24–30] and results in an increase in specific surface area [31]. Consequently, this advancement allows for an enhancement in the reaction kinetics during the desorption cycle [32–34]. In parallel, several researchers [35–39] have demonstrated that the desorption kinetics of the amorphous alloy $Mg_{50}Ni_{50}$ surpasses that of Mg_2Ni compounds.

Other researchers [40] have identified the MA method as an effective means to produce Mg-based hydrogen storage alloys. These alloys, characterized by a large surface area, exhibit reactivity with hydrogen at low temperatures and demonstrate enhanced kinetics of desorption. Yang et al. [41] reported that the synthesis of the amorphous $Mg_{50}Ni_{50}$ alloy through mechanical alloying occurs under vacuum conditions. The results obtained indicate that the random distribution of Ni and Mg atoms creates numerous tetrahedral sites in the $Mg_{50}Ni_{50}$ amorphous alloy, influencing hydrogen desorption kinetics. Additional literature [42,43] supports the observation that the desorption of hydrogen predominantly takes place during the $Mg_{50}Ni_{50}$ amorphous phase.

Sarra et al. [44] conducted an experimental study on the $Mg_{50}Ni_{50}$ amorphous alloy, revealing notable findings. The H_2 desorption content was observed to decrease from 2.3H/M at 313 K to 2.03 at 353 K, while the equilibrium pressure increased from 0.5 bar at 313 K to 1.2 bar at 353 K. In the pursuit of enhancing hydrogenation properties, numerous research studies have been undertaken and reported on metal hydrides. Among them, Mg-based hydrides have emerged as a promising candidate for hydrogen storage.

To fully explain the experimental mechanisms of hydrogen storage utilizing metal hydrides, numerous numerical studies have been undertaken across different regions globally. Advancements in research within this field have been particularly noteworthy in the 21st century. Muthukumar et al. [45] developed a 2D mathematical model using the commercial software COMSOL Multiphysics 4.2 to analyze the performance of a metal hydride-based hydrogen storage tank. They observed a high level of concordance between the numerical results and the experimental data presented in the existing literature. Whereas, Sharma et al. [46] conducted a study to examine the impacts of pressure and temperature on the thermodynamic properties of $LaNi_{4.6}Al_{0.4}$ hydride during hydrogen absorption and desorption cycles. Their investigation revealed a notable dependence of the enthalpy (ΔH) on the experimental temperature range. As well, Moropeng et al. [47] have created a C++ calculation code utilizing a numerical method for non-linear equations. This code serves to articulate the correlation between Pressure-Composition and Temperature (PCT) diagrams specific to metal hydrides of type AB_5, such as $LaNi_{4.8}Sn_{0.2}$, $LmNi_{4.91}Sn_{0.15}$, and $LaNi_{4.5}Al_{0.5}$, throughout the hydrogen storage.

Moropeng et al. [48] have constructed a two-dimensional numerical model employing the commercial software COMSOL 5.3a. This model was designed to investigate heat and mass transfer within a mixture of AB_2–AB_5 metal hydride (MH) systems. The simulation outcomes underscore the significance of the interdependence between temperature propagation within the metal hydride body, the absorbed concentration of hydrogen gas, and the gas pressure.

This paper presents the findings from both experimental and numerical studies aimed at examining the impact of elevated temperatures of the warming fluid on the phenomenon of hydrogen desorption within a cylindrical reactor containing $Mg_{50}Ni_{50}$ hydride. The investigation moreover delves into the temperature evolution and the role of cooling temperatures. To achieve this, an ample number of desorption cycles were conducted on the sample. The results revealed that both the hydrogen desorption rate and storage kinetics exhibited an increase with rising temperatures. Moreover, at elevated temperatures, the $Mg_{50}Ni_{50}$ alloy demonstrated a desorption of approximately 2% by weight of H_2. Consequently, it is evident that the cold fluid temperature significantly influences the hydrogen storage capacity.

2. Experimental detail

Based on the results obtained in previous studies, the $Mg_{50}Ni_{50}$ compound is a metal alloy of Mg (99.8%) and Ni (99.9%). The proposed sample was synthesized by using the MA method. This synthesis technique has been done using a planetary high-energy ball mill (Retch PM 200) in a stainless-steel vessel at a speed of 300 rpm for a period of 10 h. Subsequently, multiple cycles of hydrogen absorption/desorption were conducted under a pressure of approximately 15 bar and at a temperature of $T = 90\ ^\circ C$. These activation cycles were repeated until achieving a saturation value of the quantity of stored hydrogen. The XRD measurements and the internal microstructure of this sample were carried out by Sarra et al. [49] using a scanning electron microscope (SEM) and a diffractometer.

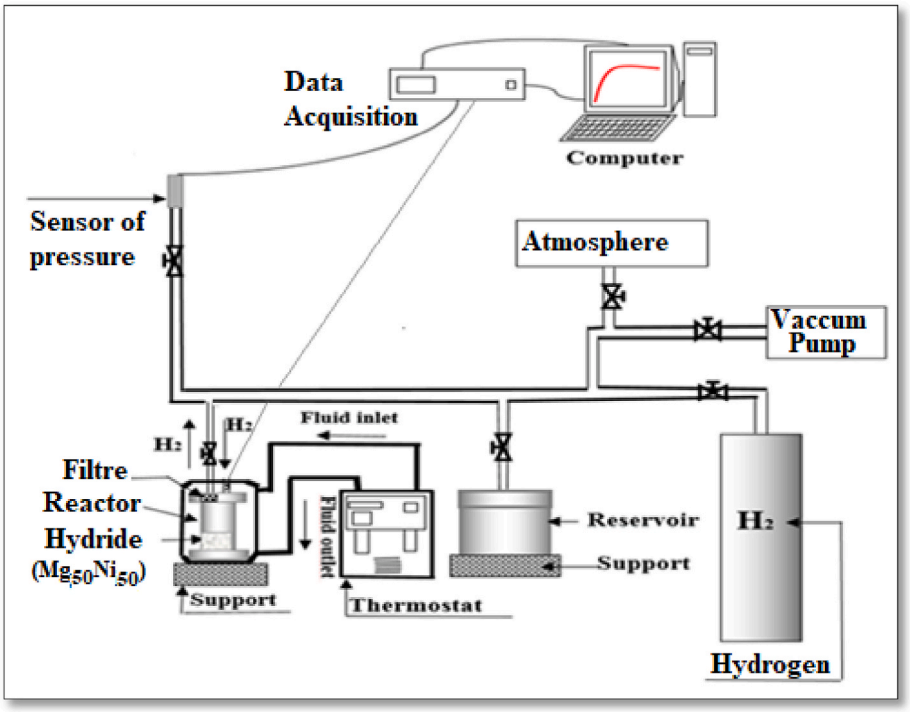

a: Schematic presentation of the experimental setup.

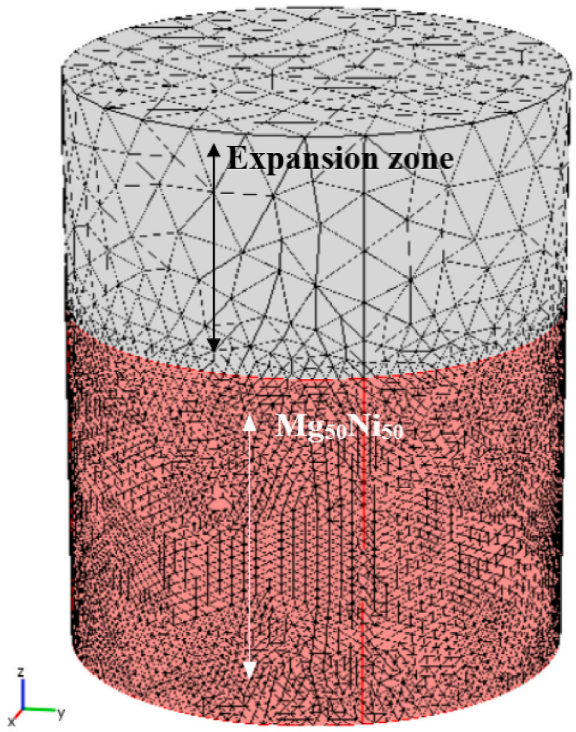

b: Schematic geometry of the simulated reactor.

Fig. 1a. Schematic presentation of the experimental setup. Schematic geometry of the simulated reactor.

Similarly, Guzmán et al. [50], have using the non-isothermal DSC experiments method under N_2 flow in an SDT 2960 apparatus (TA instruments) to study the thermal stability. More detailed information on phase evolution, and morphological study of the $Mg_{50}Ni_{50}$ alloy during the amorphization process was found in these references [51,52].

Based on the data reported in previous works [39,44], we have a good knowledge of the morphological and structural state of the $Mg_{50}Ni_{50}$ alloy. The processes of hydrogen desorption by the amorphous alloy $Mg_{50}Ni_{50}$ were measured with a Sievert-type measuring device. The experimental setup and Schematic geometry of the simulated reactor are shown in Fig. 1a and b.

To measure the temperature and the pressure (parameters of the process), it is designed to provide the desorption cycles and a data logger. The cylindrical hydrogen tank (reactor) containing the metal powder (red part on Fig. 1b), represents the principal element of the proposed device. The reactor is connected to a thermostat with the circulation of coolant fluid. The delivered water has a temperature range of 313 K–353 K. A pressure gauge measures the reservoir pressure; type PA- 21LC, 0–100 bar. A vacuum pump ensures the vacuum in the reactor and the tank. The different elements of the device are connected by valves and sealed stainless-steel tubes. The pressure evolution in the experimental device was monitored using a pressure sensor. The experimental data are recorded using an acquisition card connected to a computer.

3. Mathematical model and used assumptions

3.1. Mathematical model and geometry

Fig. 1b presents a schematic geometry of the used rector. The adsorbent bed is a half-filled cylinder with a commercial $Mg_{50}Ni_{50}$ powder (red part of the cylinder), where certain tubes pass through. The hydrogen entering the reactor in the axial direction (grey part of the cylinder). The thermophysical and geometrical parameters are presented in Table 1.

Many assumptions have been considered in developing the used model. In our case, we have supposed that the media is in the local thermal equilibrium ($T_{gas} = T_{solid}$).

On the other hand, the proposed model is used in an isotropic solid phase with uniform porosity, and the gas phase is supposed ideal. Hysteresis phenomena of the pressure-concentration isotherms are neglected in our simulation for the calculation of the Equilibrium gas pressure.

The proposed model, which describes the H_2 diffusion through the hydride bed, is based on energy balances for the hydrogen-heating model, mass balances for H_2 diffusion model, and heat exchanger metal hydride bed model. In our case, adsorption kinetics depends on pressure is taken into consideration to valid the proposed mathematical model [13–16].

Based on these assumptions, the energy balances for hydrogen heating are as follows (**Eq. (1)**):

$$\rho_{hyd} c_{p-hyd} \frac{\partial T_{hyd}}{\partial t} + \nabla \cdot \left(-\lambda_{hyd} \nabla T_{hyd} \right) = 0 \tag{1}$$

Where ρ_{hyd} is the hydrogen density, c_{p-hyd}, is the specific heat of the hydrogen, λ_{hyd}, is the thermal conductivity of the hydrogen, and T_{hyd}, is the hydrogen temperature.

The energy balances for the heat exchanger metal and the hydride bed are given by the following equations (**Eqs. 2 and 3**):

$$\rho_m c_{pm} \frac{\partial T_m}{\partial t} + \nabla \cdot (-\lambda_m \nabla T_m) = 0 \tag{2}$$

Where ρ_m is the hydride (metal) density, c_{pm}, is the specific heat of the hydride, λ_m, is the thermal conductivity of the hydride, and T_m, is the hydride temperature.

Table 1
Tank physical properties and thermodynamic parameters for the $Mg_{50}Ni_{50}$ alloy.

Parameters	Values
Hydrides bed (Re) external radius	0.02 m
Hydrides bed (L) length	0.05 m
Heating/cooling fluid velocity (v)	0.5 ms^{-1}
Initial temperature (T_0)	300K
Initial pressure (P_0)	1.5 atm
Density of the initial hydride (ρ_0)	3200 kg m-3
Density of the saturation hydride (ρ_{ss})	3240 kg m-3
Hydrides bed porosity (ε)	0.5
Specific heat of the hydride (C_{ps})	419 J kg^{-1} K^{-1}
Thermal conductivity of the hydride (λ_s)	1.2 W m^{-1} K^{-1}
Sorption enthalpy (ΔH)	17791.46 J mol-1
Hydrogen charge pressure (P_{ext})	8 atm
Cooling fluid temperature (T)	313, 333, 353 K
Ideal gas constant	8.314 (Jmol^{-}1K^{-}1)
Sorption entropy ΔS^0	51.846

$$\left[(1-\varepsilon)\rho_s c_{ps}+\varepsilon\rho_g c_{pg}\right]\frac{\partial T_s}{\partial t}+\nabla\cdot\left(-\lambda_s\nabla T_s\right)+\nabla\cdot\left(\rho_g c_{pg}T_s\overrightarrow{u}\right)=(1-\varepsilon)|\Delta H|\frac{\partial\rho_s}{\partial t} \tag{3}$$

Where ε represent the hydride bed porosity.

The mass balances for the hydride bed model are as follows (Eq. (4)):

$$\varepsilon\frac{\partial\rho_{hyd}}{\partial t}+\nabla\cdot\left(\overrightarrow{u}\rho_{hyd}\right)=-(1-\varepsilon)\frac{\partial\rho_m}{\partial t} \tag{4}$$

Moreover, to better compute the proposed model we suppose that the gas is ideal, and the hydrogen density expression is as follows (Eq. (5)):

$$\rho_{hyd}=\frac{M_{hyd}P}{RT} \tag{5}$$

Where M_{hyd} represent the hydrogen molar mass, P is the pressure, and R is the perfect gas constant.

Darcy and Van't Hoff's laws (**Eqs**. **6** and **7**) are used with Kozeny – Carman's equation (expression (**8**)) to better compute the hydride bed heat exchanger:

$$\overrightarrow{u}=-\frac{K}{\mu_g}\nabla P \tag{6}$$

$$P_{eq}=\exp\left(A-\frac{B}{T}\right) \tag{7}$$

$$K=\frac{d_p^2\varepsilon^3}{150\,(1-\varepsilon^2)} \tag{8}$$

where K, is the hydride permeability, and A, and B, are constants.

The used adsorption kinetics model is as follows (Eq. (9)):

$$\frac{\partial\rho_m}{\partial t}=Ca\exp\left(-\frac{Ea}{R\,T}\right)Ln\left(\frac{P}{P_{eq}}\right)(\rho_{ss}-\rho_m) \tag{9}$$

Where ρ_{ss} is the density of the saturation hydride, and ρ_{ss}, is the hydride (metal) density.

3.2. Boundary conditions

Based on experimental data, we have used three external temperatures as a boundary condition (Eq. (10)):

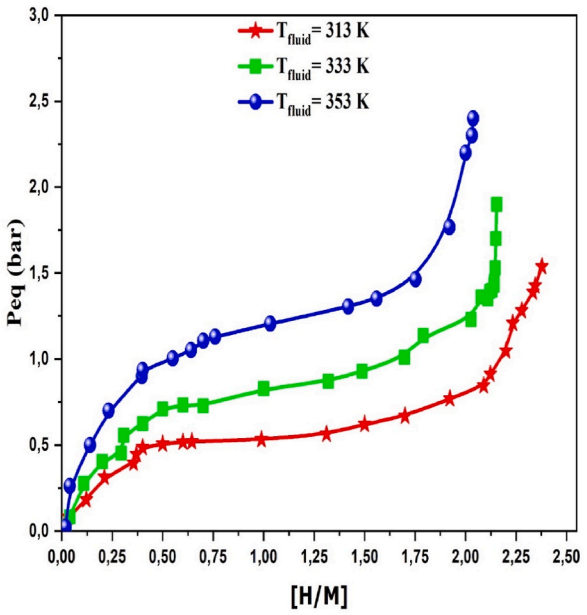

Fig. 2. Pressure–composition isotherms of the desorption state for the $Mg_{50}Ni_{50}$ alloy in a temperature range from 313 K to 353 K.

$$T_f(r = r\ \max) = 313K, 333K\ and\ 353K \tag{10}$$

At the gas-solid interface, we have used a thermal boundary resistance model a boundary condition as follows (**Eq. (11)**):

$$-\lambda_s \frac{\partial T}{\partial r}(z = \text{interface}) = hw\ (T_m - T_s) \tag{11}$$

Where *hw* represents the interface metal-hydride thermal resistance.

4. Results and discussion

4.1. PRESSURE-COMPOSITION isotherms

The studied device is presented in Fig. 1a which is investigated in a previous studies conducted by our research team [49–51] based on the volumetric method using a Sieverts–type apparatus. Before the measurement processes, 1 g of $Mg_{50}Ni_{50}$ alloy metal powder was placed in a stainless steel reactor. Several absorption-desorption cycles of hydrogen were performed at T = 323K and an initial pressure P = 15 bar for the purpose of alloy activation treatment. After 25 cycles, the amount of hydrogen absorbed stabilizes. In this case, the experimental measurements of the isotherms are carried out at three different temperatures, ranging from 313K to 353K. The principle of measurement consists of measuring the pressure (P), the composition (C), and the temperature (T), isotherms of the $Mg_{50}Ni_{50}$ alloy. Fig. 2 shows the evolution of the isotherms (P–C-T) of the $Mg_{50}Ni_{50}$ alloy in the temperature range of 313 K–353 K. The shapes of the curves provide a clear and sharp understanding of the desorption properties of the composition.

It is obvious that during the first phase (α), there is a small pressure increase due to the transformation of Mg–Ni into Mg–Ni–H. For the second phase (α+β), there is a very small increase in equilibrium pressure despite the amount of desorbed hydrogen increasing. Whereas, in the third phase (β), the equilibrium pressure increases strongly for a small increase in concentration [H/M]. In addition, the equilibrium plate increases slightly with the increase in temperature, which is attributed to the thermodynamic stability of the intermediate compositions of the alloy.

The equilibrium pressure and the temperature evolution at which the $Mg_{50}Ni_{50}$ alloy can desorb a quantity [H/M] of hydrogen is a fundamental property of the proposed metal, which is simply explained by the Van't Hoff expression given by **Eq. (12)**, which facilitates the determination of the entropy (ΔS) and the enthalpy (ΔH), of the proposed hydride.

$$\ln\left(\frac{P_{eq}}{P_0}\right) = \frac{\Delta H^0}{RT} - \frac{\Delta S^0}{R} \tag{12}$$

where: P_o is the initial pressure (1 bar H_2), P_{eq} is the equilibrium pressure, R is the perfect gas constant, T is the absolute temperature, ΔS^0 and ΔH^0 are the entropy and the enthalpy, respectively, at initial conditions associated to the desorption reaction.

Fig. 3 presents the evolution of the equilibrium pressure versus inverse of temperature. It is clear that a linear relationship was observed between ln (P_{eq}/P_0) and 1/T. From the slope of the Van't Hoff plot, the experimental value of the enthalpy of hydride formation ΔH^0 can be determined, and the order at the origin allows calculating the experimental value of the entropy. These values of ΔH^0 and ΔS^0 are listed in Table 2.

The MgH_2 hydride is known for its high during hydrogen absorption-desorption, making it less favorable in terms of thermodynamics stability. Moreover, the high ΔH harming the storage of hydrogen amount. From the values of ΔH and E_a, it is clear that the apparent ΔH value of $Mg_{50}Ni_{50}$ alloy is very low compared to the ΔH value of the MgH_2 alloy. This indicates that the heat release during the desorption of hydrogen is less significant. Therefore, less energy is required to release hydrogen, which can lead to more

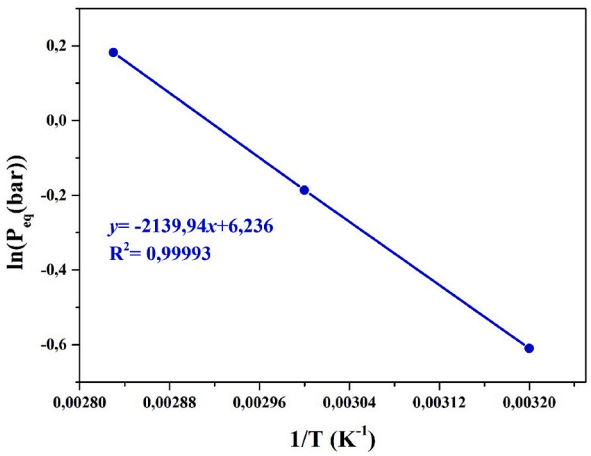

Fig. 3. Evolution of the pressures P_{eq} versus the inverse of temperatures T^{-1} for the hydrogen desorption in the $Mg_{50}Ni_{50}$ alloy.

Table 2
Thermodynamic parameters E_a, ΔH^0 and ΔS^0 for the $Mg_{50}Ni_{50}$ alloy.

R (Jmol^{-}1K^{-}1)	ΔH^0 (Jmol^{-1})	ΔS^0 (Jmol^{-1})	E_a (Jmol^{-1})
8314	**17,791,46**	**51,846**	**14,965**

energy efficient processes.

4.2. Simulation of the temperature evolution inside the hydride bed

Fig. 4 depicts the temporal temperature evolution at the contact metal hydrogen with different cooling temperature by using a mathematical approach. We show that the simulated temperatures have the same shape with different amplitude at the metal hydrogen contact. This difference is due to the role of the cooling temperature. The shown increasing is due in the fact to the hydrogen absorption process (exothermal reaction). Furthermore, after 50 s (absorption process time), the temperature achieved saturation which was caused by the cooling temperature effect.

This phenomenon is well described in Fig. 5, which illustrated the effect of cooling temperature on the temperature of the axial hydride bed during the process of the desorption phenomenon.

We show that the temperature has a maximum value in contact metal hydrogen. The adsorption phenomenon caused the increase of the system temperature. On the other hand, the cooling temperature has also an important role in the temperature increase. The temperature achieved 362K, 370K and 380K when we use a cooling temperature of 313K, 333K and 353K, respectively.

Fig. 6 depicts a 3D temperature evolution at 1000 s. From this figure, it is clearly shown that the temperature is maximal in the hydride core at the metal hydrogen interface and decreased when we move away to the tank wall.

The radial evolution of the temperature is described in Fig. 7, which presents a comparison of the temperature along the radial direction with different cooling temperatures. Due to the cooling effect, we show that the temperature decreased when we move away from the core to the tank wall.

4.3. Hydrogen desorption's kinetics

The process of desorption characteristics of the prepared composite was studied. The sample is activated after several tests with an initial hydrogen pressure applied equally to 12 bar and desorption under a vacuum of 1 bar at T = 353 K. Throughout the measurement, the cold fluid flow rate is kept constant at 13 g/l.

Fig. 8 shows the progress of the amount of desorbed hydrogen in the amorphous sample $Mg_{50}Ni_{50}$.

It is observed that the hydrogen desorption rate for the sample varies according to time and depends on the warming temperature. Based on experimental results, it can be concluded that the amount of hydrogen desorbed for the $Mg_{50}Ni_{50}$ alloy was significant at high temperatures. This suggests that the amorphous phase of the alloy improved the hydride kinetics and hydrogen storage capacity. This improvement is likely attributed to the structural and compositional properties of the amorphous phase. Furthermore, the amorphous phase exhibits favorable thermodynamic and kinetic properties for hydrogen desorption. The alloy composition and structure can influence the binding energy between hydrogen and the alloy, resulting in improved hydrogen release at elevated temperatures.

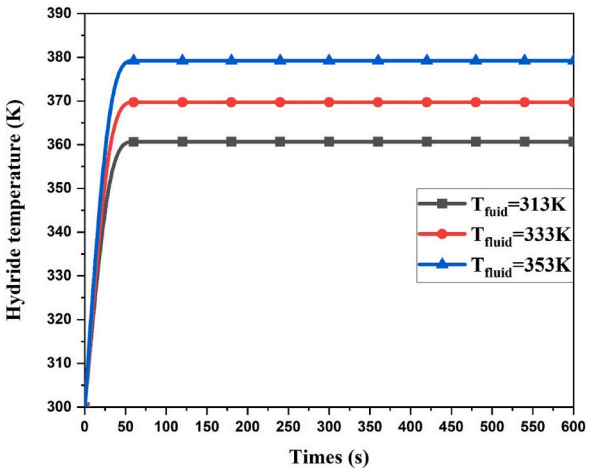

Fig. 4. Temporal temperature evolution at the metal-hydrogen contact with different cooling temperature.

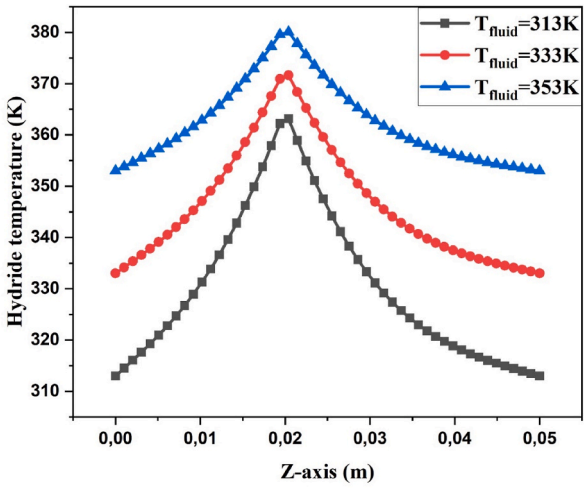

Fig. 5. Cooling temperature effect of hydride bed during the process of desorption.

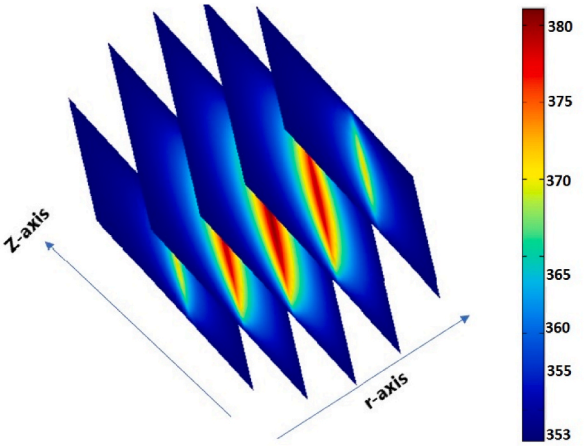

Fig. 6. 3D hydride bed temperature.

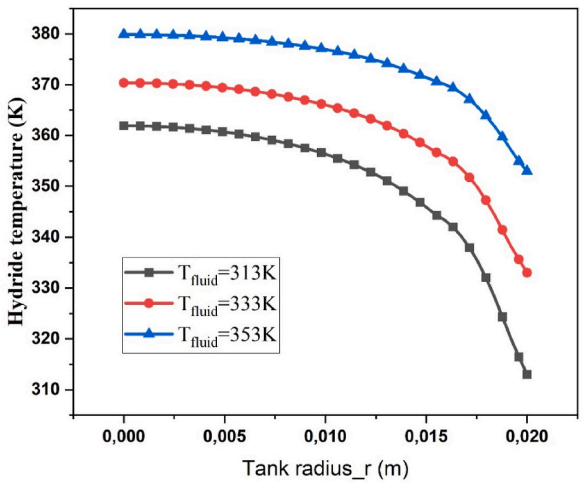

Fig. 7. Cooling temperature effect on the radial hydride bed temperature during the desorption process.

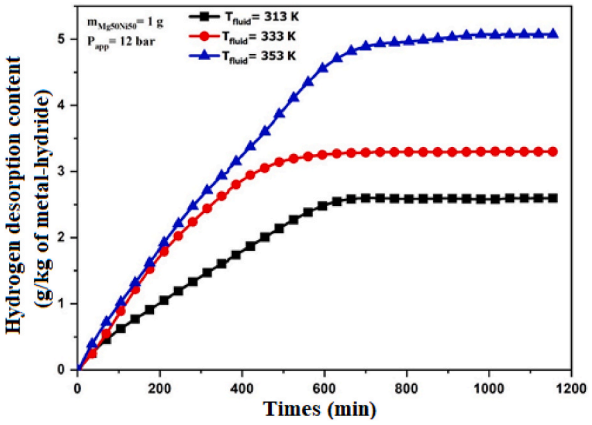

Fig. 8. Hydrogen desorption characteristics of the $Mg_{50}Ni_{50}$ alloy.

4.4. Reaction's kinetics determination

In these studies, the reaction kinetics of the $Mg_{50}Ni_{50}$ alloy were determined experimentally. During the desorption process, we put a low pressure of the order of 5 mbar in the tank. The given pressure is executed by using a vacuum pump. The recording of the evolution of the pressure in time brings us to determinate the hydride atomic ratio evolution.

In this case and assuming that r is given by an Arrhenius-type expression (**Eq. (13)**):

$$r = r_0 \exp\left(-\frac{E_d}{R_g T}\right) \tag{13}$$

Where r is the rate constant that depends on the temperature, E_d is the apparent activation energy for the state of desorption, T is the temperature and R_g is the gas constant (8.314 J $mol^{-1}K^{-1}$).

The logarithm of the rate constant, ln(r), versus the inverse temperature, (1/T), is given by Eq. (14):

$$\ln(r) = \ln(r_0) - \frac{E_d}{R_g T} \tag{14}$$

Fig. 9 shows the evolution of the desorption rate r versus the inverse of the temperature of the $Mg_{50}Ni_{50}$ alloy.

From this curve, the apparent activation energy for the desorption process was determined by adjusting the experimental values. This method involves analyzing the relationship between the natural logarithm of the desorption rate (ln(r)) and 1/T using a linear plot. The apparent activation energy provides information about the energy barrier that needs to be overcome for the desorption process to occur. It is a measure of the sensitivity of the desorption rate to changes in temperature.

Based on the experimental analysis, the estimated value of the apparent activation energy for the hydrogen desorption process of the $Mg_{50}Ni_{50}$ alloy is reported to be 14,965 ± 2 $Jmol^{-1}$. This value provides important insights into the thermodynamics and kinetics of the desorption process and highlights the energy requirements for the release of hydrogen from the alloy. This value found for the activation energy (E_d) for this alloy is less than that calculated for the parent hydride MgH_2 (120 $kJmol^{-1}$) and the Nb_2O_5-doped MgH_2 is synthesized by using the ball milling (62 $kJmol^{-1}$) [25]. The E_d for the hydrogen desorption state varies depending on the temperature. In addition, the E_d value for hydrogen desorption of the $Mg_{50}Ni_{50}$ alloy is lower than the value determined by Selvan et al. [53] for the desorption of the Mg_2NiH_4 compound (183 $kJmol^{-1}$). The observed difference in values can be attributed to the varying experimental conditions, specifically the applied hydrogen pressure and warming temperature. In the studies of Selvan et al., the analysis was based on a thermogravimetric analysis for an initial hydrogen pressure equal to 100 mbar, whereas in our case, the thermogravimetric analyses were carried out under a pressure of the order of 10 mbar and a temperature of warming equal to 353 K.

Based on the experimental results, it has been observed that the E_d value for the hydrogen desorption of the amorphous $Mg_{50}Ni_{50}$ alloy is lower than the activation energy values reported in the literature for other Mg-based compounds [53–56]. The improved desorption kinetics of the amorphous $Mg_{50}Ni_{50}$ alloy can be attributed to its unique composition and structure. The amorphous phase, with its disordered atomic arrangement, provides more accessible hydrogen diffusion pathways and facilitates faster hydrogen release. Additionally, the alloy composition and specific atomic interactions within the amorphous structure could contribute to the lower activation energy for hydrogen desorption.

5. Conclusion

Mechanical alloying (MA) synthesized an amorphous alloy, $Mg_{50}Ni_{50}$. The evolution of the isotherm of the $Mg_{50}Ni_{50}$ amorphous alloy in the temperature range of 313 K–353 K was determined experimentally. A numerical study was carried out to investigate the role of the cooling temperature on the tank temperature variation. From the experimental results found, it is possible to conclude that

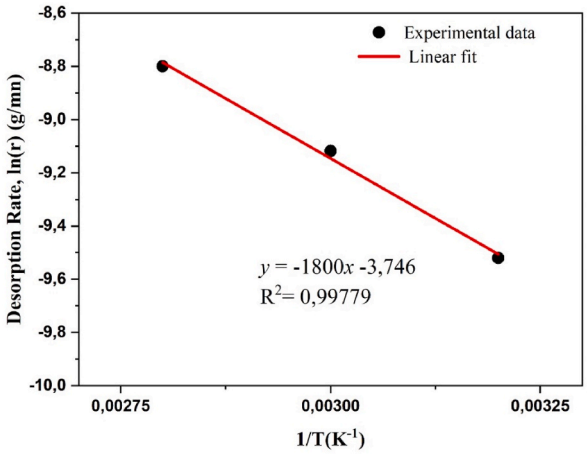

Fig. 9. The evolution of desorption rate r versus the inverse of the temperature of the $Mg_{50}Ni_{50}$ alloy.

the amorphous $Mg_{50}Ni_{50}$ improved the hydrogen storage capacity on the one hand, and kinetics desorption during the reaction on the other hand. In addition, we showed that the activation of the $Mg_{50}Ni_{50}$ alloy improves the hydrogen desorption kinetics at low heating temperatures. Similarly, we have obtained the apparent activation energy of the amorphous alloy $Mg_{50}Ni_{50}$. On the other hand, we have developed a mathematical model to investigate the tank temperature variation. We have proved that the heat conduction process is maximum at the hydride-hydrogen interface within the hydride center and decreases until it achieved the ambient at the tank walls.

CRediT authorship contribution statement

Chaker Briki: Resources, Methodology, Funding acquisition, Formal analysis, Data curation, Conceptualization. **Maha M. Almoneef:** Writing – original draft, Writing – review & editing. **Abdelhakim Settar:** Visualization, Writing – original draft, Writing – review & editing. **Mbarek Mohamed:** Formal analysis, Funding acquisition, Investigation. **Abdelmajid Jemni:** Validation, Writing – original draft, Writing – review & editing.

Declaration of competing interest

The authors declare that they have no known competing financial interests or personal relationships that could have appeared to influence the work reported in this paper.

Acknowledgements

This research was funded by Princess Nourah bint Abdulrahman University Researchers Supporting Project number (PNURSP2024R56), Princess Nourah bint Abdulrahman University, Riyadh, Saudi Arabia.

References

[1] B. Sakintuna, F. Lamari-Darkrim, M. Hirscher, Metal hydride materials for solid hydrogen storage: a review, Int. J. Hydrogen Energy 32 (2007) 1121–1140.
[2] P. Millet, 14-Hydrogen storage in hydride-forming materials, in: Advances in Hydrogen Production, Storage and Distribution, 2014, pp. 368–409.
[3] I.P. Jain, C. Lal, A. Jain, Hydrogen storage in Mg: a most promising material, Int. J. Hydrogen Energy 35 (10) (2010) 5133–5144.
[4] Á. Révész, M. Gajdics, Improved H-storage performance of novel Mg-based nanocomposites prepared by high-energy ball milling: a review, Energies 14 (19) (2021) 6400.
[5] A. Kumar, P. Muthukumar, P. Sharma, E.A. Kumar, Absorption based solid-state hydrogen storage system: a review, Sustain. Energy Technol. Assessments 52 (2022) 102204.
[6] R.S. Jin, J. Zhang, X.J. Zhou, S.X. Pan, J.H. He, J.N. Chen, X.Z. Lu, X.M. Chen, D.W. Zhou, Microstructures and hydrogen storage properties of Mg-Y-Zn rare earth magnesium alloys with different Zn content: experimental and first-principles studies, Mater. Today Commun. 32 (2022) 104119.
[7] Y. Liu, W. Zhang, X. Zhang, L. Yang, Z. Huang, F. Fang, W. Sun, M. Gao, H. Pan, Nanostructured light metal hydride: fabrication strategies and hydrogen storage performance, Renew. Sustain. Energy Rev. 184 (2023) 113560.
[8] R.C. Muduli, P. Kale, Silicon nanostructures for solid-state hydrogen storage: a review, Int. J. Hydrogen Energy 48 (4) (2023) 1401–1439.
[9] Z. Yang, K. Wang, P. Fu, L. Peng, B. Hu, M. Liu, A. Sachdev, Influence of alloying elements on hot tearing susceptibility of Mg–Zn alloys based on thermodynamic calculation and experimental, J. Magnesium Alloys 6 (1) (2018) 44–51.
[10] X. Liu, Y. Wang, W. Li, S. Wu, Q. Huang, X. Cai, L. Zhou, Preparation of Mg_2Ni hydrogen storage alloy materials with Mg-coated structure by mechanical alloying, Integrated Ferroelectrics Int. J. 234 (1) (2023) 53–66.
[11] W. Cao, X. Ding, Y. Zhang, J. Zhang, R. Chen, Y. Su, J. Guo, H. Fu, Formation of AlNi phase and its influence on hydrogen absorption kinetics of $Mg_{77}Ni_{23-x}Al_x$ alloys at intermediate temperatures, Int. J. Hydrogen Energy 47 (61) (2022) 25733–25744.
[12] D. Rahmalina, R.A. Rahman, A. Suwandi, Ismail. The recent development on MgH_2 system by 16 wt% nickel addition and particle size reduction through ball milling: a noticeable hydrogen capacity up to 5 wt% at low temperature and pressure, Int. J. Hydrogen Energy 45 (53) (2020) 29046–29058.
[13] J.S. Prasad, P. Muthukumar, Design and performance analysis of an annular metal hydride reactor for large-scale hydrogen storage applications, Renew. Energy 181 (2022) 1155–1166.

[14] F. Elhamshri, M. Kayfeci, U. Matik, S. Alous, Thermofluidynamic modelling of hydrogen absorption in metal hydride beds by using multiphysics software, Int. J. Hydrogen Energy 45 (60) (2020) 34956–34971.
[15] T. Jiahui, C. Mu, H. Kuanfang, C. Yong, Numerical simulation on heating effects during hydrogen absorption in metal hydride systems for hydrogen storage, Energies 15 (7) (2022) 2673.
[16] L. Wei, Z. Xiangguo, C. Yehui, X. Junfeng, Z. Han, W. Fang, Multi-physical thermofluidynamic simulations of hydrogen absorption performance in double-layered cylindrical ZrCo-based hydride beds, J. Appl. Phys. 130 (2021) 155101.
[17] W. Zhang, D. Zhao, Y. Zhang, J. Li, S. Guo, Y. Qi, J. Gao, Effect of Y partially substituting La on the phase structure and hydrogen storage property of La–Mg–Ni alloys, J. Phys. Chem. Solid. 167 (2022) 110744.
[18] L.Z. Ouyang, Z.J. Cao, H. Wang, J.W. Liu, D.L. Sun, Q.A. Zhang, M. Zhu, Dual-tuning effect of in on the thermodynamic and kinetic properties of Mg_2Ni dehydrogenation, Int. J. Hydrogen Energy 38 (21) (2013) 8881–8887.
[19] L. Ouyang, Z. Cao, H. Wang, R. Hu, M. Zhu, Application of dielectric barrier discharge plasma-assisted milling in energy storage materials–A review, J. Alloys Compd. 691 (2017) 422–435.
[20] L.Z. Ouyang, Z.J. Cao, H. Wang, J.W. Liu, D.L. Sun, Q.A. Zhang, M. Zhu, Enhanced dehydriding thermodynamics and kinetics in Mg(In)–MgF_2 composite directly synthesized by plasma milling, J. Alloys Compd. 586 (2014) 113–117.
[21] S. Orimo, H. Fujii, Materials science of Mg-Ni-based new hydrides, Appl. Phys. A 72 (2) (2001) 167–186.
[22] J.S. Benjamin, Dispersion strengthened superalloys by mechanical alloying, Metall. Trans. A 1 (10) (1970) 2943–2951.
[23] J.S. Benjamin, T.E. Volin, The mechanism of mechanical alloying, Metall. Trans. A 5 (8) (1974) 1929–1934.
[24] N. Singh, Y. Shadangi, V. Shivam, N.K. Mukhopadhyay, MgAlSiCrFeNi low-density high entropy alloy processed by mechanical alloying and spark plasma sintering: effect on phase evolution and thermal stability, J. Alloys Compd. 875 (2021) 159923.
[25] T. Stasiak, S.M. Aly, A. Addad, M. Touzin, F. Béclin, C. Cordier, Processing and characterization of a mechanically alloyed and hot press sintered high entropy alloy from the Al-Cr-Fe-Mn-Mo family, JOM 74 (2022) 971–980.
[26] Q. Li, Y. Lu, Q. Luo, X. Yang, Y. Yang, J. Tan, Z. Dong, J. Dang, J. Li, Y. Chen, B. Jiang, S. Sun, F. Pan, Thermodynamics and kinetics of hydriding and dehydriding reactions in Mg-based hydrogen storage materials, J. Magnesium Alloys 9 (6) (2021) 1922–1941.
[27] M.L. Huang, C.M.L. Wu, J.K.L. Lai, Y.C. Chan, Microstructural evolution of a lead-free solder alloy Sn-Bi-Ag-Cu prepared by mechanical alloying during thermal shock and aging, J. Electron. Mater. 29 (8) (2000) 1021–1026.
[28] N. Küçükdeveci, I.A. Erdoğan, A.B. Aybar, M. Anik, Electrochemical hydrogen storage properties of mechanically alloyed $Mg_{0.8}Ti_{0.2-x}Mn_xNi$ (x = 0, 0.025, 0.05, 0.1) type alloys, Int. J. Hydrogen Energy 47 (4) (2022) 2511–2519.
[29] M. Guo, H. Wang, J. Liu, L. Ouyang, Improving hydrogen-induced crystallization and electrochemical hydrogen storage properties of MgNi amorphous alloy with CoB addition, J. Non-Cryst. Solids 588 (2022) 121646.
[30] M. Taxak, N. Krishnamurthy, Effect of aluminum on hydrogen absorption kinetics of tantalum, J. Alloys Compd. 623 (25) (2015) 121–126.
[31] J. Huang, H. Wang, L. Ouyang, J. Liu, M. Zhu, Reducing the electrochemical capacity decay of milled Mg–Ni alloys: the role of stabilizing amorphous phase by Ti-substitution, J. Power Sources 438 (2019) 226984.
[32] X. Hou, Y. Wang, Y. Yang, R. Hu, G. Yang, L. Feng, G. Suo, Microstructure evolution and controlled hydrolytic hydrogen generation strategy of Mg-rich Mg-Ni-La ternary alloys, Energy 188 (2019) 116081.
[33] F. Khodabakhshi, O. Ekrt, M. Abdi, A.P. Gerlich, M. Mottaghi, R. Ebrahimi, M. Nosko, G. Wilde, Hydrogen storage behavior of Mg/Ni layered nanostructured composite materials produced by accumulative fold-forging, Int. J. Hydrogen Energy 47 (2) (2022) 1048–1062.
[34] L. Wei, Y. Zhu, L. Li, Effect of SiC on hydrogen storage properties of $Mg_{95}Ni_5$ prepared by hydriding combustion synthesis and mechanical milling, J. Alloys Compd. 539 (2012) 215–220.
[35] D. Guzmán, S. Ordoñez, J.F. Fernández, C. Sánchez, D. Serafini, P.A. Rojas, C. Aguilar, P. Tapia, Effect of amorphous $Mg_{50}Ni_{50}$ on hydriding and dehydriding behavior of Mg_2Ni alloy, Mater. Char. 62 (4) (2011) 442–450.
[36] N. Küçükdeveci, I.A. Erdoğan, A.B. Aybar, Effects of Zr addition on electrochemical characteristics of MgTiMnNi hydrogen storage alloys, Int. J. Hydrogen Energy 485 (49) (2023) 18753–18760.
[37] C. Suryanarayana, In situ mechanical crystallization of amorphous alloys, J. Alloys Compd. 961 (2023) 171032.
[38] L. Zhan, Y. Zang, Y. Zhu, X. Zhuang, N. Wan, Y. Qu, X. Guo, J. Chen, Z. Wang, L. Li, Electrochemical performances of $Mg_{45}M_5Co_{50}$ (M=Pd, Zr) ternary hydrogen storage electrodes, Trans. Nonferrous Metals Soc. China 26 (5) (2016) 1388–1395.
[39] C. Briki, S. Belkhiria, M.H. Dhaou, P. de Rango, A. Jemni, Experimental study of the influences substitution from Ni by Co, Al and Mn on the hydrogen storage properties of $LaNi_{3.6}Mn_{0.3}Al_{0.4}Co_{0.7}$ alloy, Int. J. Hydrogen Energy 42 (15) (2017) 10081–10088.
[40] D. Feng, D. Zhou, Z. Zhao, T. Zhai, Z. Yuan, H. Sun, H. Ren, Y. Zhang, Progress of graphene and loaded transition metals on Mg-based hydrogen storage alloys, Int. J. Hydrogen Energy 46 (567) (2021) 33468–33485.
[41] F. Yan, Y. Huatang, Effect of FeB doping on the structural and electrochemical characteristics of MgNi alloy, J. Alloys Compd. 473 (1–2) (2009) 275–279.
[42] J. Cermak, L. Kral, Alloying of Mg/Mg_2Ni eutectic by chosen non-hydride forming elements: relation between segregation of the third element and hydride storage capacity, J. Power Sources 197 (2012) 116–120.
[43] X. Liu, S. Wu, X. Cai, L. Zhou, Hydrogen storage behaviour of Cr- and Mn-doped Mg_2Ni alloys fabricated via high-energy ball milling, Int. J. Hydrogen Energy 48 (45) (2023) 17202–17215.
[44] S. Wjihi, C. Briki, L. Sellaoui, A. Jemni, A. Ben Lamine, Theoretical study of hydrogen desorption on $Mg_{50}Ni_{50}$ using statistical physics treatment, Int. J. Hydrogen Energy 42 (13) (2017) 8733–8743.
[45] P. Muthukumar, A. Singhal, G.K. Bansal, Thermal modeling and performance analysis of industrial-scale metal hydride based hydrogen storage container, Int. J. Hydrogen Energy 37 (19) (2012) 14351–14364.
[46] V.K. Sharma, E.A. Kumar, Effect of measurement parameters on thermodynamic properties of La-based metal hydrides, Int. J. Hydrogen Energy 39 (11) (2014) 5888–5898.
[47] M.L. Moropeng, A. Kolesnikov, M. Lototskyy, A. Mavhungu, Modelling of thermodynamic pressure – composition – temperature relationships in the systems of metallic hydride forming materials with gaseous hydrogen using C++ software, Chem. Prod. Process Model. 14 (3) (2019) 1–10.
[48] M.L. Moropeng, A. Kolesnikov, M. Lototskyy, A. Mavhungu, Numerical investigation of heat and mass transfer during hydrogen sorption in a mixture of AB_2 – AB_5 metal hydride for hydrogen storage, Chem. Prod. Process Model. 16 (1) (2020) 1–13.
[49] D. Guzmán, S. Ordoñez, D. Serafini, P.A. Rojas, C. Aguilar, M. Santander, Thermal stability of amorphous $Mg_{50}Ni_{50}$ alloy produced by mechanical alloying, J. Non-Cryst. Solids 356 (2) (2010) 120–123.
[50] H. Dhaou, A. Souahlia, S. Mellouli, F. Askri, A. Jemni, S. Ben Nasrallah, Experimental study of a metal hydride vessel based on a finned spiral heat exchanger, Int. J. Hydrogen Energy 35 (4) (2010) 1674–1680.
[51] C. Briki, S. Belkhiria, M.H. Dhaou, F. Askri, A. Jemni, Dynamic study of a new design of a tanks based on metallic hydrides, Int. J. Hydrogen Energy 43 (3) (2018) 1566–1576.
[52] C. Briki, M. Bouzid, M.H. Dhaou, A. Jemni, A. Ben Lamine, Experimental and theoretical study of hydrogen absorption by $LaNi_{3.6}Mn_{0.3}Al_{0.4}Co_{0.7}$ alloy using statistical physics modeling, Int. J. Hydrogen Energy 43 (20) (2018) 9722–9732.
[53] G. Barkhordarian, T. Klassen, R. Bormann, Effect of Nb_2O_5 content on hydrogen reaction kinetics of Mg, J. Alloys Compd. 364 (1–2) (2004) 242–246.
[54] P. Selvam, B. Viswanathan, C.S. Swamy, V. Srinivasan, Magnesium and magnesium alloy hydrides, Int. J. Hydrogen Energy 11 (3) (1986) 169–192.
[55] L. Li, T. Akiyama, J.I. Yagi, Activation behaviors of Mg_2NiH_4 at different hydrogen pressures in hydriding combustion synthesis, Int. J. Hydrogen Energy 26 (10) (2001) 1035–1040.
[56] J. Senegas, M.Y. Song, M. Pezat, B. Darriet, Phase characterization and hydrogen diffusion study in the Mg-Ni-H system, J. Less Common Metals 129 (1987) 317–326.